Journal of Membrane Science 652 (2022) 120490

Contents lists available at ScienceDirect

Journal of Membrane Science

journal homepage: www.elsevier.com/locate/memsci

# Single-walled carbon nanotube buckypaper as support for highly permeable double layer polyamide/zeolitic imidazolate framework in nanofiltration processes

Victor Berned-Samatán [a,b], César Rubio [a,b], Alejandro Galán-González [a,b], Edgar Muñoz [c], Ana M. Benito [c], Wolfgang K. Maser [c], Joaquín Coronas [a,b], Carlos Téllez [a,b,*]

[a] Instituto de Nanociencia y Materiales de Aragón (INMA), CSIC-Universidad de Zaragoza, Zaragoza, 50018, Spain
[b] Chemical and Environmental Engineering Department, Universidad de Zaragoza, Zaragoza, 50018, Spain
[c] Instituto de Carboquímica (ICB-CSIC), Zaragoza, 50018, Spain

ARTICLE INFO

*Keywords:*
Carbon nanotube
Zeolitic imidazolate framework
Nanofiltration
Polyamide membrane
Interfacial polymerization

ABSTRACT

The development of membranes for nanofiltration applications requires not only selective layers but also suitable supports to control their synthesis as well as to enable efficient and competitive membrane performances. Single-walled carbon nanotube free-standing films (denoted as buckypaper) have been used as supports for the preparation of polyamide (PA) layers by interfacial polymerization (IP) and tested for dead-end nanofiltration for dyes removal (265–1017 Da) from water and organic solvents. The arrangement of the phases during the IP is essential, thus impregnation on the buckypaper support, first with the organic phase and then with the aqueous phase (denoted as inverse IP, iIP) leads to permeances (of up to 28.0 and 31.4 L $m^{-2}$ $h^{-1}$ $bar^{-1}$ for water and methanol, respectively) and rejection values (>96%) that exceed those of the membranes prepared by reversing the impregnation order. Secondly, a double layer PA/zeolitic imidazolate framework (ZIF-8 or ZIF-93) was prepared on the buckypaper (bp). The design of this double layer led to superior membrane performance, in particular for the hydrophilic ZIF-93, as it changes the PA layer properties (increasing both hydrophilicity and surface roughness) providing higher permeances (up to 59.3 and 76.0 L $m^{-2}$ $h^{-1}$ $bar^{-1}$ for water and methanol, respectively) and dye rejections (>98.5%) than the bare PA layer prepared by iIP. This attractive performance of the PA/ZIF-93/bp membrane has been corroborated with experiments in cross-flow nanofiltration and dead-end nanofiltration of aqueous salt solutions, long-term stability nanofiltration and the study the membrane separation performance after a chlorine treatment. The results reported here therefore show the enormous potential of these membrane architectures for a variety of selective separation processes.

## 1. Introduction

Nanofiltration (NF) is a membrane separation process of solutes with molecular weights ranging between 200 and 1000 Da [1]. NF is gaining great importance in chemical industry, food industry, pharmaceutical, wastewater treatment, solvent recovery and desalination, since it is a flexible, low-cost and energy efficient process for the treatment of aqueous and organic solvent feeds [1,2]. The most common and competitive membranes in both water nanofiltration and organic solvent nanofiltration (OSN) are the so-called thin film composite (TFC) membranes [3] where the selective layer is a polyamide (PA) thin film synthesized via interfacial polymerization (IP) [4,5]. IP is usually carried out by a polycondensation reaction between *m*-phenylenediamine (MPD) in water and trimesoyl chloride (TMC) in hexane, forming a thin PA layer at the interface of the immiscible solutions [6]. Alternatively, IP can be carried out supplying the TMC from the vapor phase, without any organic solvent [7].

An improvement in membrane performance can be achieved with fillers inside the TFC membrane resulting in thin film nanocomposite (TFN) membranes [8]. Several nanoparticles can be used for such purpose: zeolites [8], $TiO_2$ [9], silica [10], graphene oxide (GO) [11], carbon nanotubes (CNTs) [12], covalent organic frameworks (COFs) [13] and metal organic frameworks (MOFs) [14]. In the TFN membrane, the lack of control in the incorporation of the filler can cause agglomerations

* Corresponding author. Instituto de Nanociencia y Materiales de Aragón (INMA), CSIC-Universidad de Zaragoza, Zaragoza, 50018, Spain.
*E-mail address:* ctellez@unizar.es (C. Téllez).

https://doi.org/10.1016/j.memsci.2022.120490
Received 10 December 2021; Received in revised form 25 February 2022; Accepted 21 March 2022
Available online 24 March 2022

and defects.

Other strategy to improve the performance of TFC membranes consists of the application of an interlayer of a porous material between the support and the PA layer, such as PA/MOF on polyimide supports [15,16] or PA/2D MOF on poly(ether sulfone) (PES) [17] or PA/base CNTs on PES [18,19]. The improvements achieved with such strategies are related to changes in the PA layer properties (thickness, surface roughness, hydrophilicity or crosslinking), a gutter layer effect (increased permeation avoiding geometric restrictions of the support due to its porosity and pore size) [20] and better control of the IP process.

The manufacture of efficient membranes requires a support that, in addition to the necessary mechanical robustness, has the suitable porous structure and surface properties since both affect the structural features and the quality of the selective layer to be grown on top [21]. Typically, TFC membranes for NF and OSN processes comprise a non-woven support at the bottom and a polymeric (e.g. polysulfone, polyethersulfone or polyimide) asymmetric porous layer where the PA thin film is supported. These supports have low porosity, rough surface and high tortuosity, which limits the achievement of selective thin layers by IP as well as their performance in nanofiltration processes [22]. These hindrances can be addressed with the use of a support or the commented intermediate layer based on nanomaterials. In particular, the high porosity, low surface roughness, low tortuosity, and uniform pore size distribution that result from the use of nanofibrous structures such as CNTs in the fabrication of supports, together with the intrinsic remarkable mechanical strength and chemical inertness of CNTs [18,21,23], favor the controlled interaction of the phases involved in the IP and lead to improved nanofiltration performances.

MOFs are crystalline materials formed by metal ionic clusters and organic linkers. MOFs exhibit high surface area and tunable and flexible pore structure, which allows affinity for polymeric chains due to their organic-inorganic chemical composition and excludes certain molecules based on their size, shape and polarity [24,25]. In this work, zeolitic imidazolate frameworks (ZIFs) ZIF-8 and ZIF-93 were used as MOFs. ZIF-8 consists of a metal cation of $Zn^{2+}$ coordinated with 2-methylimidazolate, forming a SOD type zeolitic topology with cavities of 1.16 nm connected through a pore window of 0.34 nm [26]. ZIF-93 is another $Zn^{2+}$ based MOF with 4-methyl-5-imidazolatecarboxaldehyde as the organic linker which increases hydrophilicity compared to ZIF-8. It has the RHO type zeolitic topology and cavities of 1.58 nm connected by pore window of 0.37 nm [27].

In this work, a unique membrane architecture is proposed in which a PA layer was placed directly on a single-walled carbon nanotube self-standing film (denoted as SWCNT buckypaper, CNT-bp) support. This support offers a smooth surface as well as high chemical stability and mechanical robustness. In addition, it can improve the contact between the organic and aqueous phases that contain the monomers during IP, affecting the physical-chemical properties of the PA layer and, as a consequence, the nanofiltration performance. In this work, the CNT-bp support was used, for the first time, to grow a ZIF layer onto which a PA layer was synthesized by IP to build a complex membrane suitable for nanofiltration. Clarifying the question of the importance of the order in which the phases should be added in the IP, we reveal that the ZIF layer remarkably can change the PA layer properties to obtain outstanding improvements in the application to nanofiltration processes for dyes or salt removal.

## 2. Experimental

### 2.1. Materials

Single-walled carbon nanotubes (SWCNT, 1.2–2 nm) ≥93 carbon content, non-ionic surfactant Triton™ X-100, *m*-phenylenediamine (MPD, 99%) and 1,3,5-benzenetricabonyl trichloride (TMC 98%) were purchased from Sigma-Aldrich. 2-Propanol (HPLC grade, ≥99.9%) and methanol (HPLC grade, ≥99.9%) were purchased from Panreac Applichem and n-hexane (extra pure) and zinc nitrate hexahydrate (reagent grade) were purchased from Scharlab. 4-methyl-5-imidazolecarboxaldehyde (99%) and 2-methylimidazole (99%) are from Acros Organics. Acetone (99%). Cellulose membrane filter with a diameter of 90 mm and a 290 μm thickness were purchased from Labbox. The following dyes were used for NF: rose Bengal (RB, Sigma Aldrich, 95% dye content), sunset yellow (SY, Sigma Aldrich, 90% dye content), and acridine orange (AO, Acros Organics, 55% dye content). Sodium hypochlorite solution (6–14% active chlorine) was purchased from Merck. Sodium chloride (>99%), sodium sulphate (>99%), and magnesium chloride (>99%) were purchased from Sigma-Aldrich. All the chemicals were used without any purification.

### 2.2. Preparation of single-walled carbon nanotube buckypaper (SWCNT-bp)

Free standing single-walled CNT films (SWCNT-bp), ca. 15 μm in thickness, were made by a vacuum filtration method previously reported [28]. Typically, 100 mg of SWCNT were dispersed in 300 mL of a water solution containing 1 wt% of Triton X-100 surfactant. This suspension was prepared using an ultrasonic probe sonicator (GEX750 ultrasonic processor, 750 W, 20 KHz) for 1 h, then filtered through a cellulose filter in a 90 mm in diameter glass filtration equipment, and washed with a mixture of 2-propanol and acetone [29]. The film was dried overnight at room temperature; after what it could be peeled off from the filter obtaining a 15 μm thick self-standing SWCNT film.

### 2.3. ZIF-8 and ZIF-93 MOF synthesis on SWCNT-bp

This synthesis was carried out modifying a previously reported method [30]. The free standing SWCNT-bp was placed between two metal rings to prevent one of their sides from the solutions. For the ZIF-8 synthesis (ZIF-8/SWCNT-bp), the SWCNT-bp support was placed vertically in a 10 mM zinc nitrate hexahydrate methanolic solution for 30 min. Afterwards, it was rinsed in pure methanol for 1 min, then placed vertically in a 20 mM 2-methylimidazole methanolic solution for 24 h and then rinsed in pure methanol for 1 min. This procedure was performed twice, after what the membrane was removed from the metal rings and rinsed with pure methanol for 10 min and dried overnight at room temperature. All the synthesis steps were applied at room temperature.

The same procedure was carried out for the ZIF-93 MOF (ZIF-93/SWCNT-bp) preparation with the substitution of the 2-methylimidazole solution for a 20 mM 4-methyl-5-imidazolecarboxaldehyde methanolic solution.

### 2.4. Preparation of TFC membranes

The TFC membranes were prepared following two different methods [31,32] by the IP reaction of 2% MPD aqueous solution and 0.1% TMC hexane solution. First a 60 $cm^2$ circular support was placed in a glass filtration holder.

For the conventional IP reaction at room temperature (25 °C), 20 mL of the MPD aqueous solution was added, and after 2 min the solution was removed and the membrane dried with tissue paper. Next, 20 mL of the TMC n-hexane solution was added and let react for 1 min. Then 10 mL of fresh n-hexane was added to stop the reaction and immediately removed from the support. Then the membrane was cleaned with fresh n-hexane and deionized water. The membrane was removed from the glass holder and stored in deionized water in the fridge for testing within 48 h of preparation.

For the inverse IP (iIP) reaction at room temperature (25 °C) the support was soaked in fresh n-hexane for 10 min before being placed in the glass holder. Then 20 mL of the TMC hexane solution was added and let for 5 min. Then the solution was removed and the membrane dried.

Then 20 mL of the MPD aqueous solution was added and let react for 2 min. Once the solution was removed the membrane was cleaned with fresh n-hexane and deionized water and stored in deionized water in the fridge for testing within 48 h of preparation.

These two described methods were used for the PA layer preparation on the SWCNT-bp. From here the membrane prepared with the conventional method will be labelled TFC membrane and the membrane prepared with the reverse procedure iIP TFC membrane. The inverse IP (iIP) reaction was used on the ones with the ZIFs to get PA/ZIF-8/SWCNT-bp and PA/ZIF-93/SWCNT-bp.

### 2.5. Characterization

X-ray diffraction (XRD) measurements were performed with an Empyrean PANalytical diffractometer with a Cu–K source (λ = 1.5406 Å). Data were collected in the 2θ range from 2.5° to 40° at a scanning rate of 0.01°·s$^{-1}$.

XPS experiments were conducted with a Kratos Axis Ultra spectrometer using an Al Kα (1486.6 eV) source at 8 mA and 15 kV and a power of 120 W.

Scanning electron microscope (SEM) images were collected with a FEI-Inspect F50 microscope at a voltage of 10 kV. The samples were previously coated with Au/Pd under vacuum conditions.

Attenuated total reflection - Fourier transform infrared spectroscopy (ATR-FTIR) was carried out in a Bruker Vertex 70 FTIR spectrometer with a DTGS detector and a Golden Gate diamond ATR accessory in the 600-4000 cm$^{-1}$ wavenumber range with a resolution of 4 cm$^{-1}$.

Atomic force microscopy (AFM) characterization was performed using a Veeco MultiMode 8 scanning probe microscope in tapping mode at a scan rate of 1 Hz and amplitude lower than 1 V under ambient conditions.

Water contact angle measurements were carried out using a Krüss DSA 10 MK2 at 25 °C. Three measures of each membrane were performed to obtain an average water contact angle value.

More details about the characterization techniques used in this work as well as their usefulness in the evaluation of membranes for filtration processes can be found in the literature [7,11,15,32–35].

### 2.6. Nanofiltration experiments

The nanofiltration process was performed at room temperature (25 °C) and 10 bar feed pressure under continuous stirring in a dead-end membrane module (Sterlitech HP4750) and in a cross-flow filtration installation (see more details in [36]) with a flat membrane effective area of 12 cm$^2$. The performance was evaluated using 250 mL feeds of 20 mg L$^{-1}$ of rose Bengal (RB), sunset yellow (SY) and acridine orange (AO) in distilled water and 250 mL feeds of 20 mg L$^{-1}$ of the same dyes in MeOH for the dead-end experiments and 1 L min$^{-1}$ feed flow of a 20 mg L$^{-1}$ of RB aqueous solution for the cross-flow experiments. In dead-end nanofiltration, the membranes were kept under pressure for 1 h, when stable values were reached the measurement was performed, usually in about 3 h. It should be noted that when the volume of the dead-end module was at 20% capacity, the solution was renewed. In cross-flow nanofiltration the measurement was performed when stable values were reached, usually in about 6 h.

The dyes removal is of interest for the treatment of wastewater from textile, paint, leather and paper processing industries where large volumes of polluted effluents are produced [37]. In methanol, these dyes allow for an easy comparison of their performance in an organic solvent. They also serve as model for testing the behavior of these membranes in OSN [38], being used for the recovery of organic solvents especially in pharmaceutical industries.

The same membrane was used for the three colorants in the order RB, SY and AO first in methanol and then in water. All the experiments were carried out at a feed pressure of 10 bar. The rejection and the permeance were calculated by equations (1) and (2):

$$Rejection(\%) = \left(1 - \frac{C_{permeate}}{C_{residue}}\right) x100 \quad (1)$$

$$Permeance = \frac{V}{\Delta P \cdot A \cdot t} \quad (2)$$

where, A is the area of the membrane (m$^2$), t is the time for permeate collection (h), V is the volume collected at time t (L) and ΔP is the pressure difference (bar) used in the experiments between the retentate and permeate.

The concentration of both the permeate ($C_{permeate}$) and the residue ($C_{residue}$) were measured by an UV spectroscopy (JASCO V-670 spectrophotometer) using water as a solvent at a wavelength of 549 nm for RB, 480 nm for SY and 490 nm for AO. In the case of the MeOH feed, 3 mL of the permeate and the residue were evaporated and replaced with 3 mL of deionized water.

Salt rejection was also studied in the dead-end membrane module with 250 mL feeds of 1.0 g L$^{-1}$ solutions of $Na_2SO_4$, NaCl and $MgCl_2$. The concentration of both the permeate and the residue were determined by electric conductivity meter (Mettler Toledo Seven Multi) and its salt rejection and permeance calculated with equations (1) and (2).

The chlorine resistance of membrane was studied. As reported in literature, short time exposure of membranes to high concentrations of chlorine are similar to long time exposure to low concentrations of chlorine [39]. The membrane performances were tested with the dead-end membrane module at room temperature (25 °C), 10 bar feed pressure and 250 mL feeds of 1.0 g L$^{-1}$ $Na_2SO_4$ solution or 20 mg L$^{-1}$ of RB aqueous solution, then immersed into a 1000 ppm sodium hypochlorite (NaOCl, pH 4) solution for 1 h. After washing thoroughly with distilled water, the separation performance was measured again.

The long-term filtration performance was evaluated for the PA/ZIF-93/SWCNT-bp membrane in the cross-flow filtration installation for 80 h with a 1 L min$^{-1}$ feed flow of 20 mg L$^{-1}$ RB aqueous solution.

## 3. Results and discussion

### 3.1. PA Layer on SWCNT-bp supports: effect of the arrangement of the aqueous and organic phases during IP

TFC membranes without MOF layers were prepared on top of SWCNT-bp supports following two different procedures as described in the experimental section. The conventional IP where the support is impregnated first with the aqueous solution of the MPD monomer, and then with the organic phase containing the TMC monomer. Alternatively, inverse IP (iIP) was carried out by impregnation in a TMC hexane solution, followed by impregnation in a MPD aqueous solution. SEM characterization indicates that the synthesized PA layers exhibit the rough surface morphologies typical of PA TFC membranes as shown in Fig. 1 [40].

Regarding the characterization, bands at 1619 cm$^{-1}$ (C═O), 1546 cm$^{-1}$ (C–N) and 1453 and 1410 cm$^{-1}$ (–NHCO–) in ATR-FTIR spectra (Fig. 2) further confirms the growth of PA layers. In Fig. 3, the water contact angle (CA) is not very different for the two TFC membranes (CA = 70° and CA = 67° for the membranes synthesized with IP and iIP, respectively). Nevertheless, both TFC membranes show more hydrophilic surface than the SWCNT-bp support (CA = 83°).

Dead-end nanofiltration performance (permeance and dye rejection) was evaluated filtering solutions of three dyes of different molecular weight: namely RB (1017 Da), SY (452 Da) and AO (265 Da) in water for nanofiltration (NF) and in methanol for organic solvent nanofiltration (OSN). The SWCNT-bp support has a permeance higher than 1000 L m$^{-2}$ h$^{-1}$ bar$^{-1}$ with no observable rejection. Fig. 4 A, B shows the performance comparison between the two different syntheses of the PA layer over the bare SWCNT-bp support. These results show a clear improvement in the permeance of the iIP PA layer in the water dead-end

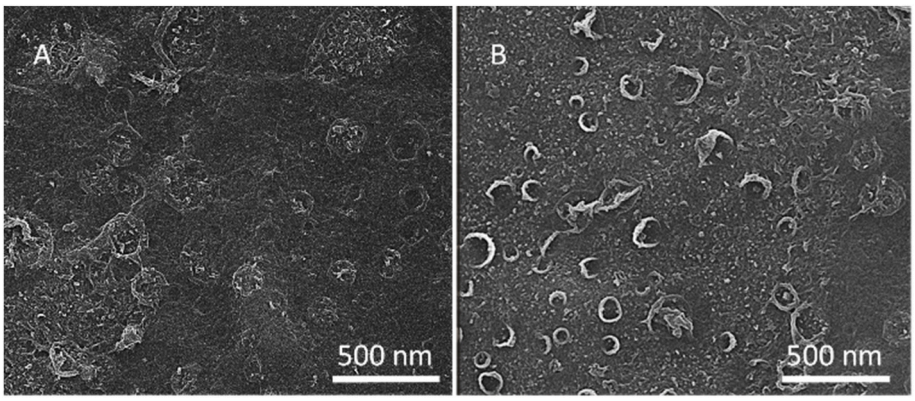


**Fig. 1.** SEM images of surface membranes: A) TFC. B) iIP TFC.

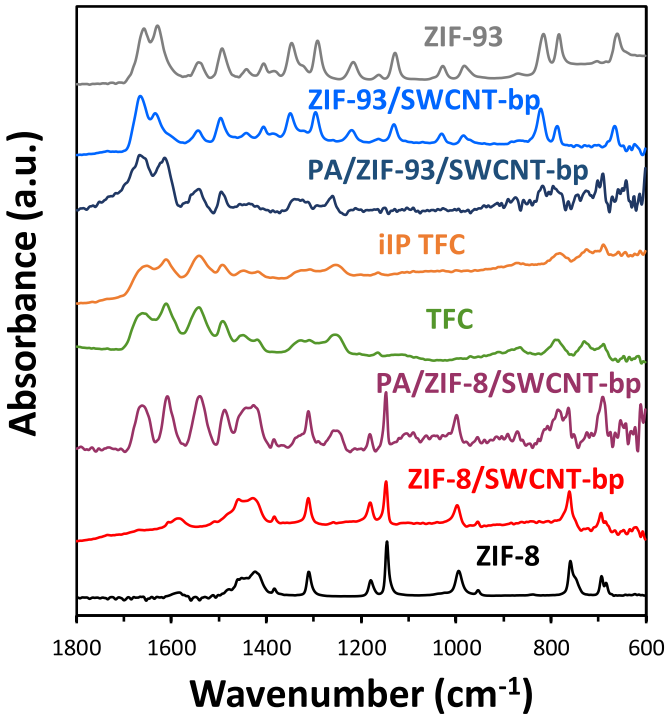


**Fig. 2.** Normalized ATR-FTIR spectra of MOFs and different membranes subtracting the SWCNT-bp support spectrum.

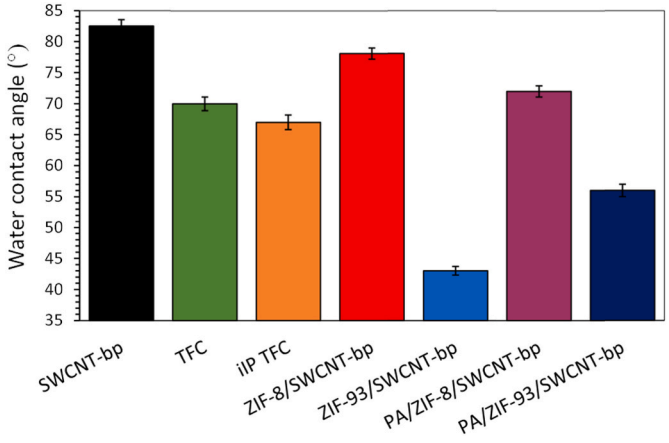


**Fig. 3.** Water contact angle of the synthetized membranes.

NF and also in the dead-end OSN with maximum permeances of 28.0 ± 3.3 L $m^{-2}$ $h^{-1}$ $bar^{-1}$ (water) and 32.2 ± 5.1 L $m^{-2}$ $h^{-1}$ $bar^{-1}$ (methanol), respectively, when compared to the 3 ± 1.4 L $m^{-2}$ $h^{-1}$ $bar^{-1}$ (water) and 8 ± 3 L $m^{-2}$ $h^{-1}$ $bar^{-1}$ (methanol) obtained with the conventional IP method. Regarding permeances, the experiments carried out in cross-flow nanofiltration of RB aqueous solution (Fig. 4A) and dead-end NF of aqueous solutions of salts (Fig. 4C) show similar trends to the dead-end nanofiltration experiments with dyes (Fig. 4A and B). The dyes rejections were similar in water dead-end NF for the two synthesis methods with more than 96% rejection for all the three dyes, whilst in dead-end OSN there is again a noteworthy improvement with the iIP synthesis method increasing the rejections from 88.0 ± 2.5% (RB), 85.5 ± 3.5% (SY) and 86.7 ± 1.3% (AO) to 98.5 ± 2.8% (RB), 97.0 ± 3.5% (SY) and 96.9 ± 2.9% (AO). These nanofiltration results clearly indicate the higher quality of the PA layer synthesized by iIP, revealing a molecular weight cut-off (MWCO, solute of lower molecular weight in which 90% of the solute is retained by the membrane) of at least 265 Da in both methanol and water nanofiltrations. The above MWCO value must be taken with caution since the interaction of the dyes may compromise its correct determination.

The comparison of these two procedures (conventional and iIP) has already been reported for other membrane supports with frequently contradictory results given their diverse nature in terms of structure and hydrophobic/hydrophilic character [41]. These results are commonly explained in terms of the growth of dense PA layers formed at the water-hexane interface and loose or less cross-linking PA layers that grow in the organic phase [42]. To unravel it, the XPS characterization of the surface of the TFC and iIP TFC membranes has been carried out. Table 1 shows an increase in the C/N and O/N ratios for the iIP TFC membrane with respect to the conventional TFC membrane which would indicate the XPS analysis penetration into the SWCNT-bp support and a lower degree of cross-linking of the PA layer, respectively. It should be noted that the O/N ratio can be influenced by the support and therefore cross-linking considerations should be taken with caution, furthermore, the O/N value below one in the conventional TFC membrane may be related to the fact that more MPD participates in the IP to form the PA layer [43]. The noted trends can be related to the fact that the dense PA layer on the support is thinner with good quality in the iIP TFC membrane respect the TFC membrane where the PA layer would be thicker and of lower quality due to the worse contact of the hydrophobic SWCNT-bp support with the aqueous solution which is added first in this case. In addition, the PA is growing loosely inside the support of iIP TFC membrane where is the hexane phase. This agrees with the observation done by Wang et al. [44] who performed a analogous study on a 250 nm cellulose nanofiber layer, with a surface structure that resembles that of the SWCNT-bp supports used here. On the other hand, the TMC solution is more diluted thus the amount stored in the support and available for reaction after impregnation with first solution of TMC (iIP) must be

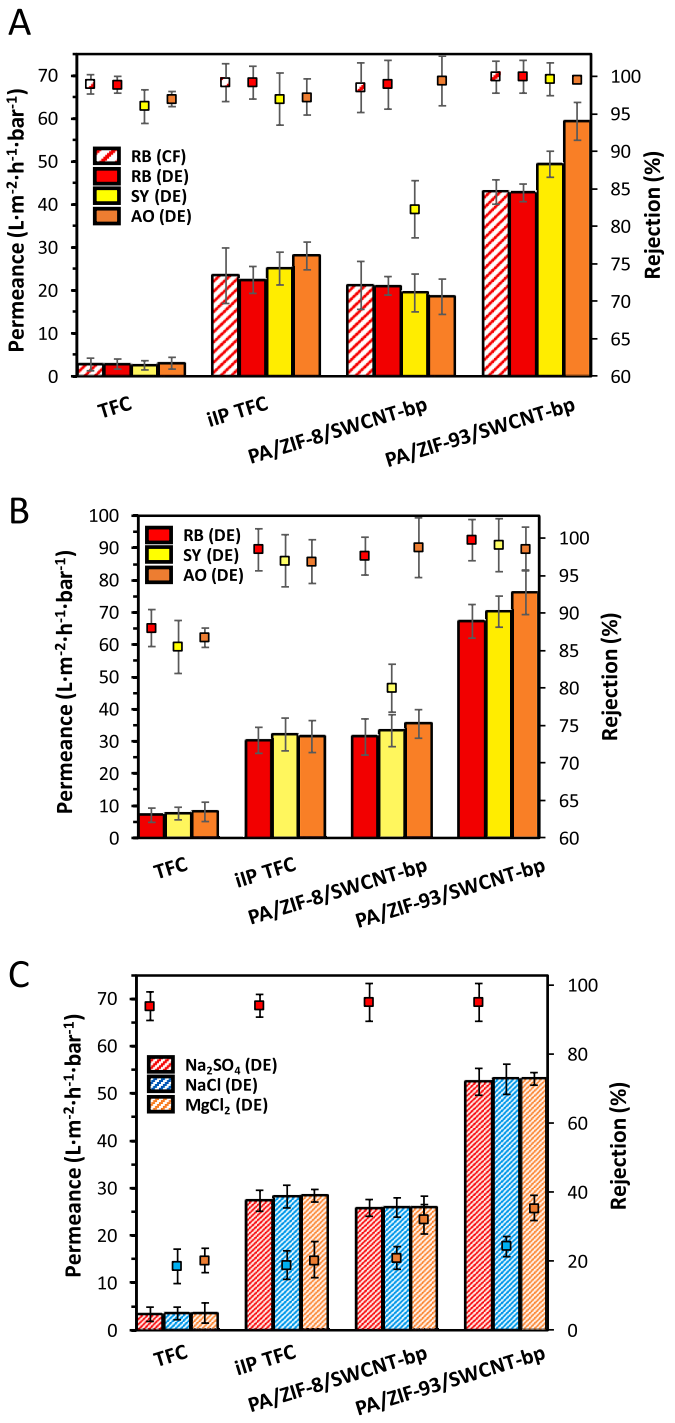


**Fig. 4.** Permeance (bars) and dye rejection (dots) comparison of membranes: A) Dead-end (DE) and cross-flow (CF) NF of dye aqueous solutions. B) Dead-end (DE) OSN of dye solutions in methanol. C) Dead-end (DE) NF of aqueous solutions of salts. Values are in Tables S1, S2, S3 and S4. Conditions: 25 °C and 10 bar feed pressure. Dyes: AO, SY an RB. The error bars come from the measurement of three different membrane samples.

much smaller than for MPD impregnated first (conventional IP). This will undoubtedly decrease the IP reaction rate and thus the thickness of the polyamide layer in the iIP, in agreement with similar reactant concentration effects previously reported [45]. All commented factors favor dye rejection and permeance in the iIP TFC membrane.

**Table 1**
C/N and O/N atomic ratios obtained through the quantification of C, N and O elements from XPS analysis.

| Membrane | % Zn | C/N | O/N |
|---|---|---|---|
| TFC | 0 | 5.1 ± 0.1 | 0.6 ± 0.1 |
| iIP TFC | 0 | 15.0 ± 1.7 | 1.3 ± 0.1 |
| PA/ZIF-8/SWCNT-bp | 0.8 ± 0.2 | 11.2 ± 0.6 | 1.1 ± 0.1 |
| PA/ZIF-93/SWCNT-bp | 0.4 ± 0.1 | 11.3 ± 0.7 | 1.0 ± 0.1 |

### 3.2. Double layer polyamide/zeolitic imidazolate framework

The crystallization of ZIF layers prior to IP on SWCNT-bp support was carried out modifying a previously reported method as described in the experimental section. SEM images of ZIF8/SWCNT-bp and ZIF-93/SWCNT-bp (Fig. 5A, C) show intergrown layers with both ZIF-8 and ZIF-93 with an estimated thickness of ca. 50 nm. For this type of membranes where a PA layer is synthetized on top of a MOF layer, the MOF layer could be rather loose (as evaluated by gas permeation testing) [16], modifying the support surface but not hindering the permeation. XRD pattern of the ZIF-8 and ZIF-93 layers show the majority of the characteristic peaks of the MOF (Fig. 6). MOF characteristic FTIR bands (Table S5) shown in Fig. 2 further confirm the growth of ZIF-8 and ZIF-93 layers.

The iIP PA synthesis was then chosen for the synthesis of a PA layer on top of ZIF-8/SWCNT-bp and ZIF93/SWCNT-bp membranes. The surface of both PA/ZIF/SWCNT-bp membranes (Fig. 5B, D) is very similar to that of the TFC membranes (Fig. 1). The amorphous layer of PA masks the characteristic X-ray diffraction peaks (not shown) of the ZIFs. On the other hand, the ATR-FTIR spectra of both membranes (Fig. 2) show the characteristic peaks of PA bands mentioned above, as well as most of the bands corresponding to each ZIF.

Regarding XPS characterization of PA/ZIF/SWCNT-bp membranes (Table 1), the C/N ratio and the presence of Zn indicate that the analysis penetrates both ZIF layers. The C/N ratios are slightly lower than in the iIP-TFC membrane, due to the presence of nitrogen in the ZIF structure where the polyamide layer grows. MOF containing membranes showed a slightly decreased of O/N ratio which could indicate an increase in the cross-linking of the PA layer with respect to de iIP TFC. Even though we see an increase in permeance, as will be shown later, this is in agreement with previously studies where this increase in crosslinking does not have to mean a decrease in permeance as indicated by Van Goethem et al. [46], who discussed that the HCl released during the PA condensation could degrade part of the MOF structure releasing $Zn^{2+}$. These Zn ions produce a permeance enhancement even though the cross-linking increased. In any case, the C/N and O/N ratios in the two ZIF membranes are very similar, their performance in NF being very different as will be seen below, which seems to indicate that there are another effects that influence the separation ability of the membranes.

A marked difference between the characterized membranes lies on their hydrophilicity, as shown in Fig. 3. The CA of the pristine SWCNT-bp support decreases by the addition of the ZIF layer. The ZIF-8/SWCNT-bp membrane fully reflects the inherent hydrophilic nature of ZIF-8 and thus exhibits the highest CA value of all the coated membranes. On the other hand, the hydrophilic character of ZIF-93 leads to the membrane with the lowest CA value. When the PA layer is synthetized, the CA values for both PA/ZIF-8/SWCNT-bp and PA/ZIF-93/SWCNT-bp membranes lie between those of their respective ZIF/SWCNT-bp and TFC membranes. Therefore, ZIF-93-containing membranes exhibited higher hydrophilicity, that leads to enhanced water or methanol permeance, as it will be discussed later.

AFM images (Fig. 7) and derived average roughness (Ra) and root mean square roughness (RMS) (Table S6) show an increase in the roughness of the surface in the order SWCNT-bp < iIP TFC < ZIF-93/SWCNT-bp < PA/ZIF-93/SWCNT-bp. The increase in roughness when the ZIF-93 is used to synthesize the PA layer ($R_a = \pm 297$) compared with

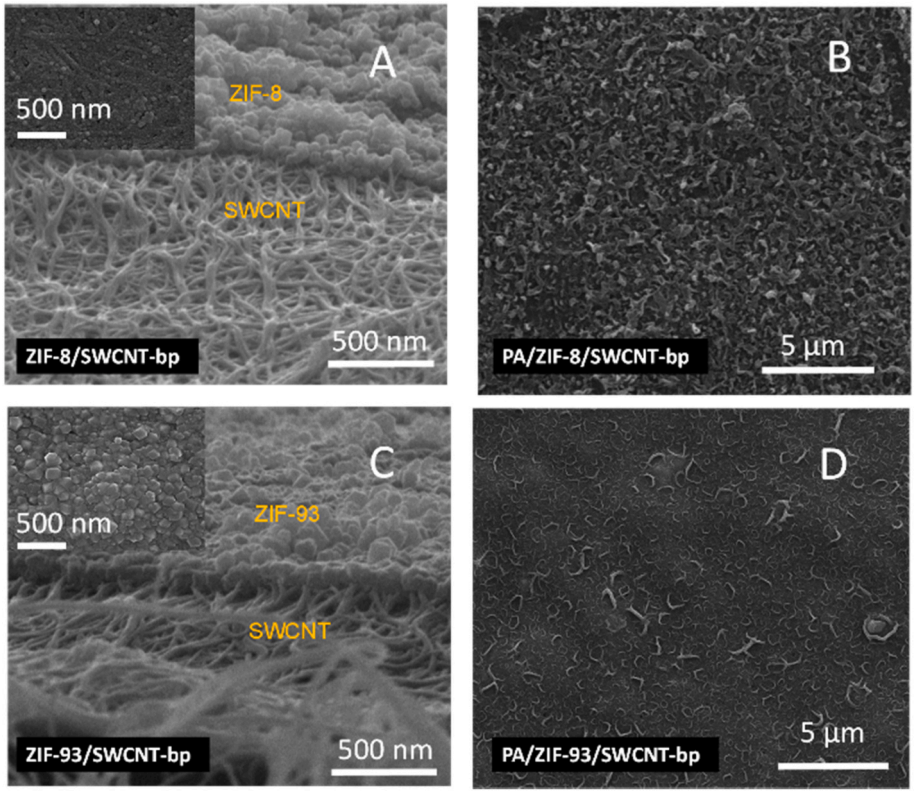


**Fig. 5.** SEM images of membranes: A) Cross-section of ZIF-8/SWCNT-bp with inset of surface. B) Surface of PA/ZIF-8/SWCNT-bp. C) Cross-section of ZIF-93/SWCNT-bp with inset of surface. D) Surface of PA/ZIF-93/SWCNT-bp.

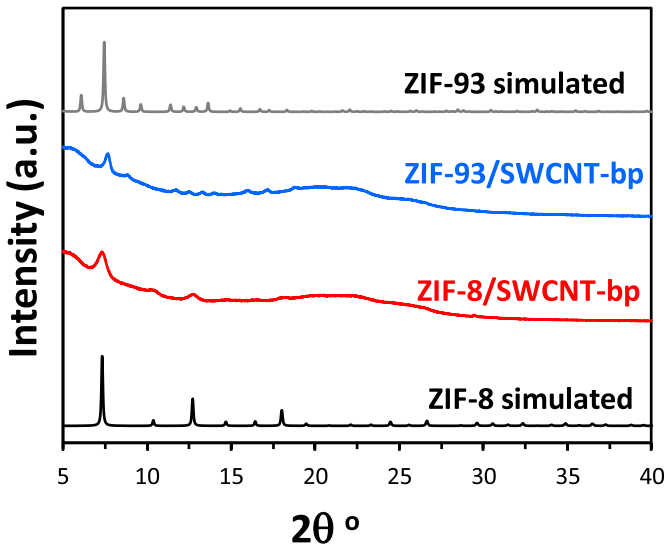


**Fig. 6.** Normalized XRD patterns of MOF layers together with its simulated patterns.

the one of iIP TFC ($R_a = \pm 192$) is in agreement with the literature [15]. Greater roughness is often associated with higher effective surface area, which plays a key role increasing the permeance and, therefore, it is consistent with the permeance results achieved for the ZIF-93-containing membranes tested here.

Similarly to TFC membranes, PA/ZIF-8/SWCNT-bp and PA/ZIF-93/SWCNT-bp membranes were tested using dead-end nanofiltration for RB, SY and AO dye solutions in water and methanol. Fig. 4A and B shows that the PA/ZIF-8/SWCNT-bp membrane provides maximum permeances of 21.0 ± 2.2 L $m^{-2}$ $h^{-1}$ $bar^{-1}$ and 35.4 ± 4.5 L $m^{-2}$ $h^{-1}$ $bar^{-1}$ for water and methanol solutions, respectively, these values being very close to those achieved with the TFC membrane synthesized by iIP. This could be related to the similar hydrophilic nature exhibited by both the SWCNT-bp support (CA = 83°) and the ZIF-8/SWCNT-bp membrane (CA = 78°), which leads to similar contact of the organic and aqueous phases during the synthesis of the PA layer. On the other hand, when the PA layer is synthetized on ZIF-93/SWCNT-bp (more hydrophilic with CA = 43°), the PA/ZIF-93/SWCNT-bp membrane shows remarkable permeance improvements in comparison to the bare iIP TFC membrane with maximum permeances of 59.3 ± 4.4 L $m^{-2}$ $h^{-1}$ $bar^{-1}$ and 76.0 ± 6.8 L $m^{-2}$ $h^{-1}$ $bar^{-1}$ for water and methanol solutions, respectively. The more hydrophilic character of the PA/ZIF-93/SWCNT-bp membrane (CA = 56°) also favours the transport of polar solvents more than the PA/ZIF-8/SWCNT-bp membrane (CA = 73°). In any event, the ZIF-93 layer has a gutter layer effect avoiding the penetration of the IP reactants into the SWCNT-bp support during the synthesis and thus generating a thin and permeable selective skin layer that in turn is more hydrophilic.

In comparison with iIP TFC membrane, rejections also show an increase with the PA/ZIF-93/SWCNT-bp membrane reaching 99.9 ± 2.2% (RB), 99.6 ± 2.3% (SY), 99.5 ± 2.4% (AO) for NF and 99.7 ± 2.8% (RB), 99.1 ± 3.5% (SY) and 98.6 ± 2.9% (AO) for OSN. These increases may be related to a higher degree of crosslinking related to the presence of the MOF layer that also has the indicated gutter layer effect, as previously reported [17]. It should be noted that the rejection for SY dye (82.3 ± 3.8 for NF and 80.0 ± 3.2 for OSN) with the PA/ZIF-8/SWCNT-bp membrane is lower than that of the AO dye (99.4 ± 3.3 for NF and 98.7 ± 4.0 for OSN) which has a smaller molecular weight. This effect is not observed in iIP TFC and PA/ZIF-93/SWCNT-bp membranes where rejections are usually always greater than 97%. This suggests that the ZIF-8 layer may affect the surface charge of the PA layer giving rise to a better rejection of the cationic dyes such as AO as

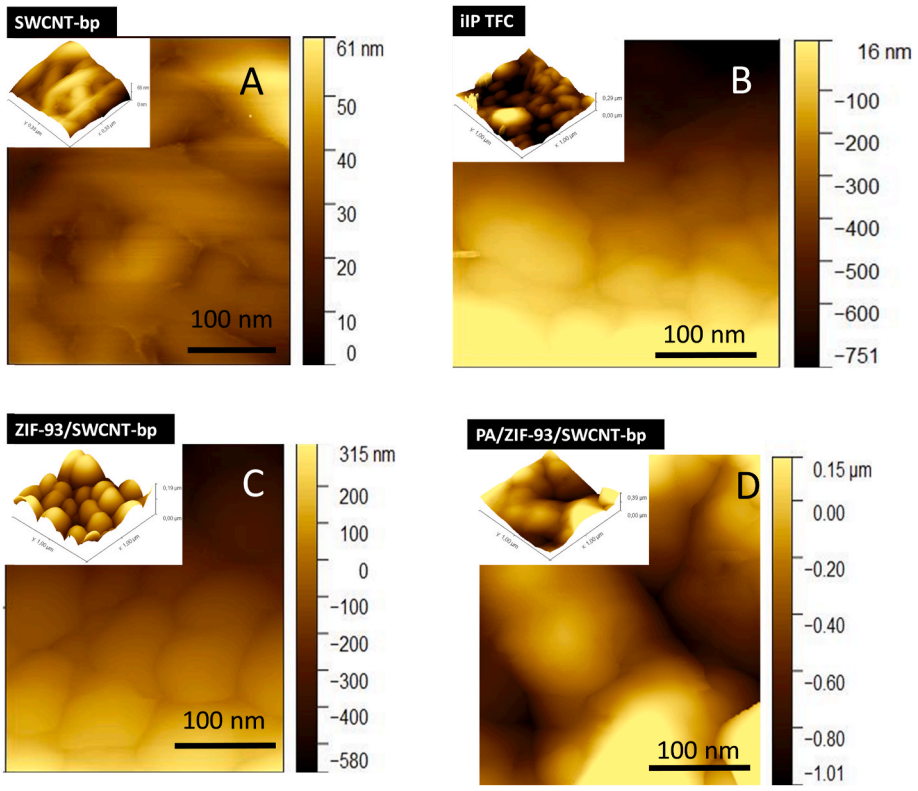


**Fig. 7.** AFM images of membranes: A) SWCNT-bp (Ra = 50 ± 2.0). B) iIP TFC (Ra = 133 ± 2 nm). C) ZIF-93/SWCNT-bp (Ra = 192 ± 2 nm). D) PA/ZIF-93/SWCNT-bp (Ra = 297 ± 3 nm).

compared to the anionic dyes such as SY and RB regardless of their molecular size. In case of the PA/ZIF-93/SWCNT-bp membrane, the dye rejection is related to the molecular weight of the dye which is in accordance with different properties of the PA layer on ZIF-93 than on ZIF-8. In any case, the PA/ZIF-93/SWCNT-bp membrane shows rejections greater than 98.5% for the AO molecule. This indicates, with the precautions noted above, that this membrane has a MWCO of at least 265 Da in both methanol and water.

Cross-flow nanofiltration was also carried out filtering RB aqueous solution until the results were stable which resulted in a duration of the experiment of 6 h. Fig. 4A shows that the RB nanofiltration results are almost identical with dead-end and cross-flow, which confirms the reliability of the observed trends and results.

Salt rejection experiments were also carried out in the dead-end filtration installation (Fig. 4C). The permeance values and the trends with the type of membrane are very similar to those obtained in the nanofiltration of the dyes. Membranes show a good performance for the nanofiltration of $Na_2SO_4$ always reaching salt rejection values greater than 94%. The best values are located again with the PA/ZIF-93/SWCNT-bp membrane reaching a permeance of 52.5 ± 2.8 L $m^{-2}$ $h^{-1}$ $bar^{-1}$ and a $Na_2SO_4$ rejection of 95.0 ± 4.9%. For the rest of the salts, a noticeable drop in the rejection can be observed with values of 24.3 ± 2.9% for the NaCl and 35.4 ± 3.7% for the $MgCl_2$ in the ZIF-93 containing membrane. In the literature it has been reported that Donnan exclusion and size exclusion mechanisms may play a role in nanofiltration performance [47]. Our results agree with the tendency observed in literature for salt rejection ($Na_2SO_4 \geq MgCl_2 \geq NaCl$) that can be related to the Donnan effect, leading to a greater rejection for high valent anions like $Na_2SO_4$ [48].

A long-term experiment to test the stability of the membrane, Fig. 8, was carried out for the best performing membrane PA/ZIF-93/SWCNT-bp in the cross-flow filtration installation for a total duration of the experiment of 80 h. This experiment showed a great stability of the membrane over time with almost no drop in both permeance (42.7 L $m^{-2}$ $h^{-1}$ $bar^{-1}$) and RB rejection (99.9%).

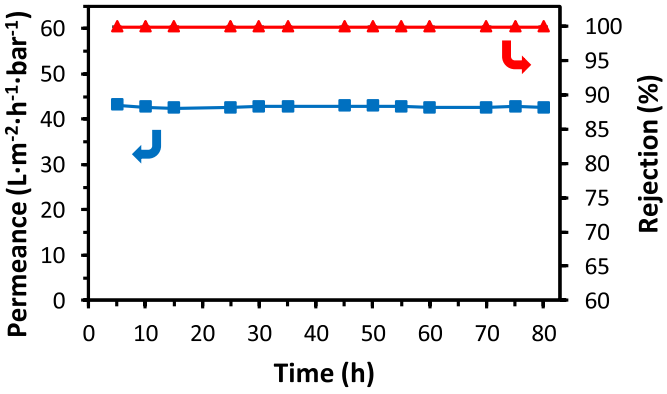


**Fig. 8.** Permeance (blue) and dye rejection (red) of the PA/ZIF-93/SWCNT-bp membrane for the nanofiltration of rose Bengal (RB) in water for 80 h in the cross-flow filtration installation. Conditions: 25 °C and 10 bar feed pressure. (For interpretation of the references to color in this figure legend, the reader is referred to the Web version of this article.)

Chlorine stability experiments, Fig. 9, were carried out with all the membranes, tested for the $Na_2SO_4$ salt and the RB dye, showing a good stability after being in contact for 1 h with a 1000 ppm NaOCl solution. It can be seen a slightly increase in the permeance and a decrease in the rejection but always within the corresponding error values. The effect is a little more marked with the salt. These results are in agreement with the literature where the membrane chlorination leads to an increase in permeance while the variation in rejection depends on the properties of the solute [49]. In any case, the PA/ZIF-93/SWCNT-bp membrane shows a stability comparable to that of the TFC membranes, which opens the door to the practical use of these much more permeable and selective membranes.

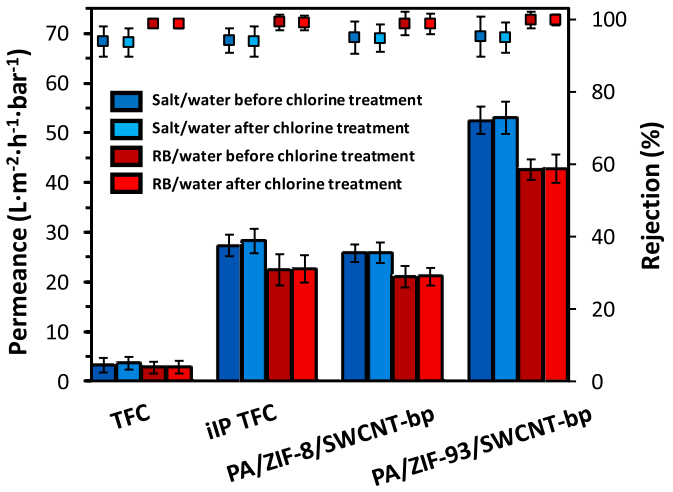


**Fig. 9.** Permeance (bars) and dye rejection (dots) of the membranes for the dead-end nanofiltration of $Na_2SO_4$ and RB before and after being treated with NaOCl (1000 ppm, pH 4) for 1 h. Values are in Tables S7 and S8. Conditions: 25 °C and 10 bar feed pressure. The error bars come from the measurement of three different membrane samples.

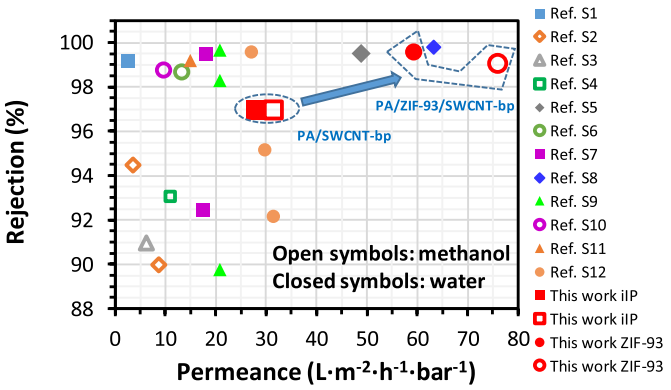


**Fig. 10.** Performance comparison between this study and other works using PA membranes based on MOFs or CNT on the removal of different dyes from water or methanol (data from Table S9).

Fig. 10 summarizes a comparison of the best membranes synthesized in this work with those chosen from the literature based on MOF or CNT and used for nanofiltration of dyes. The conditions in which the nanofiltration is carried out in the data of Table S9 vary since different solvents (water or methanol) are used as well as different dyes that have different molecular weight and charge. Considering these limitations of the comparison, it is important to point out that the membranes reported here are undoubtedly among the best reported in terms of both permeance and dye rejection, even without the addition of a ZIF layer. Furthermore, whenever possible, the permeance ratio of the polyamide membrane with ZIF or CNT with respect to the polyamide membrane without ZIF or CNT is also indicated in Table S9. This relationship allows evaluating the permeance improvement as a result of the growth of a ZIF layer. For the membranes of this work, these ratios lie between 2.1 and 2.4, which are of the same order as those corresponding to other high performance membranes, with the advantage that in general the permeances and rejections are higher for the membranes reported here, which further highlights their potential for application in dye removal processes and, in general, in nanofiltration.

## 4. Conclusions

In summary, a membrane architecture is proposed here to form composite membranes based on the fabrication of a PA layer on SWCNT supports via two different methods: conventional IP and inverse IP (iIP). Precise control of the IP process is achieved with the iIP method which offers superior performances for nanofiltration for dye removal from both wastewater and methanol. The permeances and rejections achieved with this PA layer are among the best in the literature, which indicates the success of using CNTs as support to obtain highly permeable and defect-free PA layers. The best results of iIP respect to conventional IP are related to the good contact between the phases and the support during the IP and the lower thickness of the polyamide layer achieved.

The nanofiltration results were further improved upon the growth of hydrophilic ZIF-93 layers on SWCNT-bp supports prior to the synthesis of the PA film. To discern the cause of the enhancements, membranes have been characterized by a number of techniques including XRD, XPS, ATR-FTIR, contact angle, SEM, and AFM. The ZIF-93 layer modifies the IP process and the properties (particularly hydrophilicity measured by water contact angle and surface roughness measured by AFM) of the resulting membrane providing narrow solvent paths giving rise to the highest performance in terms of permeance and rejection for dye removal by nanofiltration from both wastewater and solvent methanol. The trends and excellent behavior of the PA/ZIF-93/SWCNT-bp membrane have been corroborated with experiments in cross-flow and dead-end nanofiltration of dyes as well as dead-end nanofiltration of salts in water.

The PA/ZIF-93/SWCNT-bp membrane has been shown to be stable in performance (permeance and dye rejection) for 80 h in a cross-flow nanofiltration process. In addition, the membrane was as stable to chlorine treatment as membranes with only polyamide supported on SWCNT-bp.

The PA/MOF double layer on SWCNT-bp supports opens the door to progress towards highly permeable and selective membranes, choosing the appropriate MOF and rendering these membranes candidates for other separation processes such as reverse osmosis or even gas separation.

## Author statement

**Víctor Berned:** Investigation, Methodology, Validation, Formal analysis, Visualization, Writing - Original Draft, Writing - Review & Editing.

**Cesar Rubio:** Methodology, Formal analysis, Writing - Original Draft.

**Alejandro Galán-González:** Investigation, Formal analysis, Writing - Original Draft.

**Edgar Muñoz:** Conceptualization, Methodology, Supervision, Funding acquisition, Writing - Original Draft.

**Ana M. Benito:** Conceptualization, Methodology, Supervision, Funding acquisition, Writing - Original Draft.

**Wolfgang K. Maser:** Conceptualization, Methodology, Supervision, Funding acquisition, Writing - Original Draft.

**Joaquín Coronas:** Conceptualization, Methodology, Supervision, Funding acquisition, Writing - Original Draft, Writing - Review & Editing.

**Carlos Téllez:** Conceptualization, Methodology, Supervision, Funding acquisition, Writing - Original Draft, Writing - Review & Editing.

## Declaration of competing interest

The authors declare that they have no known competing financial interests or personal relationships that could have appeared to influence the work reported in this paper.

## Acknowledgements

Grants PID2019-104009RB-I00 and PID2019-104272RB-C51 funded

by MCIN/AEI/10.13039/501100011033 are gratefully acknowledged (Agencia Estatal de Investigación (AEI) and MCIN (Ministerio de Ciencia e Innovación), Spain). The Aragón Government is also gratefully acknowledged (Grupos reconocidos T43_20R, T03_20R and E25_20R). V. B.-S. thanks the Grant BES-2017-080209 funded by MCIN/AEI/10.13039/501100011033 and by "ESF Investing in your future". The authors would like to acknowledge the use of the Servicio General de Apoyo a la Investigación-SAI and the use of instrumentation as well as the technical advice provided by the National Facility ELECMI ICTS, node "Laboratorio de Microscopias Avanzadas" at the University of Zaragoza.

## Appendix A. Supplementary data

Supplementary data to this article can be found online at https://doi.org/10.1016/j.memsci.2022.120490.

## References

[1] P. Marchetti, M.F.J. Solomon, G. Szekely, A.G. Livingston, Molecular separation with organic solvent nanofiltration: a critical review, Chem. Rev. 114 (21) (2014) 10735–10806, https://doi.org/10.1021/cr500006j.
[2] S.T. Muntha, A. Kausar, M. Siddiq, Advances in polymeric nanofiltration membrane: a review, Polym. Plast. Technol. Eng. 56 (8) (2017) 841–856, https://doi.org/10.1080/03602559.2016.1233562.
[3] R.J. Petersen, Composite reverse-osmosis and nanofiltration membranes, J. Membr. Sci. 83 (1) (1993) 81–150, https://doi.org/10.1016/0376-7388(93)80014-o.
[4] P. Vandezande, L.E.M. Gevers, I.F.J. Vankelecom, Solvent resistant nanofiltration: separating on a molecular level, Chem. Soc. Rev. 37 (2) (2008) 365–405, https://doi.org/10.1039/b610848m.
[5] I. Soroko, M.P. Lopes, A. Livingston, The effect of membrane formation parameters on performance of polyimide membranes for organic solvent nanofiltration (OSN): Part A. Effect of polymer/solvent/non-solvent system choice, J. Membr. Sci. 381 (1–2) (2011) 152–162, https://doi.org/10.1016/j.memsci.2011.07.027.
[6] M. Paul, S.D. Jons, Chemistry and fabrication of polymeric nanofiltration membranes: a review, Polymer 103 (2016) 417–456, https://doi.org/10.1016/j.polymer.2016.07.085.
[7] L. Paseta, C. Echaide-Gorriz, C. Tellez, J. Coronas, Vapor phase interfacial polymerization: a method to synthesize thin film composite membranes without using organic solvents, Green Chem. 23 (6) (2021) 2449–2456, https://doi.org/10.1039/d1gc00236h.
[8] B.H. Jeong, E.M.V. Hoek, Y.S. Yan, A. Subramani, X.F. Huang, G. Hurwitz, A. K. Ghosh, A. Jawor, Interfacial polymerization of thin film nanocomposites: a new concept for reverse osmosis membranes, J. Membr. Sci. 294 (1–2) (2007) 1–7, https://doi.org/10.1016/j.memsci.2007.02.025.
[9] D. Emadzadeh, W.J. Lau, T. Matsuura, M. Rahbari-Sisakht, A.F. Ismail, A novel thin film composite forward osmosis membrane prepared from PSf-TiO2 nanocomposite substrate for water desalination, Chem. Eng. J. 237 (2014) 70–80, https://doi.org/10.1016/j.cej.2013.09.081.
[10] J. Yin, E.S. Kim, J. Yang, B.L. Deng, Fabrication of a novel thin-film nanocomposite (TFN) membrane containing MCM-41 silica nanoparticles (NPs) for water purification, J. Membr. Sci. 423 (2012) 238–246, https://doi.org/10.1016/j.memsci.2012.08.020.
[11] L. Paseta, J.M. Luque-Alled, M. Malankowska, M. Navarro, P. Gorgojo, J. Coronas, C. Tellez, Functionalized graphene-based polyamide thin film nanocomposite membranes for organic solvent nanofiltration, Separ. Purif. Technol. 247 (2020) 116995, https://doi.org/10.1016/j.seppur.2020.116995.
[12] M. Amini, M. Jahanshahi, A. Rahimpour, Synthesis of novel thin film nanocomposite (TFN) forward osmosis membranes using functionalized multi-walled carbon nanotubes, J. Membr. Sci. 435 (2013) 233–241, https://doi.org/10.1016/j.memsci.2013.01.041.
[13] J.Q. Yuan, M.Y. Wu, H. Wu, Y.A. Liu, X.D. You, R.N. Zhang, Y.L. Su, H. Yang, J. L. Shen, Z.Y. Jiang, Covalent organic framework-modulated interfacial polymerization for ultrathin desalination membranes, J. Mater. Chem. 7 (44) (2019) 25641–25649, https://doi.org/10.1039/c9ta08163a.
[14] J. Campbell, R.P. Davies, D.C. Braddock, A.G. Livingston, Improving the permeance of hybrid polymer/metal-organic framework (MOF) membranes for organic solvent nanofiltration (OSN) - development of MOF thin films via interfacial synthesis, J. Mater. Chem. 3 (18) (2015) 9668–9674, https://doi.org/10.1039/c5ta01315a.
[15] M. Navarro, J. Benito, L. Paseta, I. Gascon, J. Coronas, C. Tellez, Thin-film nanocomposite membrane with the minimum amount of MOF by the Langmuir-schaefer technique for nanofiltration, ACS Appl. Mater. Interfaces 10 (1) (2018) 1278–1287, https://doi.org/10.1021/acsami.7b17477.
[16] C. Echaide-Gorriz, J.A. Zapata, M. Etxeberria-Benavides, C. Tellez, J. Coronas, Polyamide/MOF bilayered thin film composite hollow fiber membranes with tuned MOF thickness for water nanofiltration, Separ. Purif. Technol. 236 (2020) 116265, https://doi.org/10.1016/j.seppur.2019.116265.
[17] Y. Wen, X.R. Zhang, X.S. Li, Z.W. Wang, C.Y. Tang, Metal-organic framework nanosheets for thin-film composite membranes with enhanced permeability and selectivity, ACS Appl. Nano Mater. 3 (9) (2020) 9238–9248, https://doi.org/10.1021/acsanm.0c01860.
[18] M.B. Wu, Y. Lv, H.C. Yang, L.F. Liu, X. Zhang, Z.K. Xu, Thin film composite membranes combining carbon nanotube intermediate layer and microfiltration support for high nanofiltration performances, J. Membr. Sci. 515 (2016) 238–244, https://doi.org/10.1016/j.memsci.2016.05.056.
[19] S.J. Gao, Y.Z. Zhu, Y.Q. Gong, Z.Y. Wang, W.X. Fang, J. Jin, Ultrathin polyamide nanofiltration membrane fabricated on brush-painted single-walled carbon nanotube network support for ion sieving, ACS Nano 13 (5) (2019) 5278–5290, https://doi.org/10.1021/acsnano.8b09761.
[20] M. Kattula, K. Ponnuru, L.X. Zhu, W.G. Jia, H.Q. Lin, E.P. Furlani, Designing ultrathin film composite membranes: the impact of a gutter layer, Sci. Rep. 5 (2015) 15016, https://doi.org/10.1038/srep15016.
[21] Y.Z. Zhu, W. Xie, S.J. Gao, F. Zhang, W.B. Zhang, Z.Y. Liu, J. Jin, Single-walled carbon nanotube film supported nanofiltration membrane with a nearly 10 nm thick polyamide selective layer for high-flux and high-rejection desalination, Small 12 (36) (2016) 5034–5041, https://doi.org/10.1002/smll.201601253.
[22] Z.Y. Zhou, Y.X. Hu, Q. Wang, B.X. Mi, Carbon nanotube-supported polyamide membrane with minimized internal concentration polarization for both aqueous and organic solvent forward osmosis process, J. Membr. Sci. 611 (2020) 118273, https://doi.org/10.1016/j.memsci.2020.118273.
[23] V.N. Popov, Carbon nanotubes: properties and application, Mater. Sci. Eng. R Rep. 43 (3) (2004) 61–102, https://doi.org/10.1016/j.mser.2003.10.001.
[24] P. Falcaro, R. Ricco, C.M. Doherty, K. Liang, A.J. Hill, M.J. Styles, MOF positioning technology and device fabrication, Chem. Soc. Rev. 43 (16) (2014) 5513–5560, https://doi.org/10.1039/c4cs00089g.
[25] S. Sorribas, P. Gorgojo, C. Tellez, J. Coronas, A.G. Livingston, High flux thin film nanocomposite membranes based on metal-organic frameworks for organic solvent nanofiltration, J. Am. Chem. Soc. 135 (40) (2013) 15201–15208, https://doi.org/10.1021/ja407665w.
[26] M. Etxeberria-Benavides, T. Johnson, S. Cao, B. Zornoza, J. Coronas, J. Sanchez-Lainez, A. Sabetghadam, X.L. Liu, E. Andres-Garcia, F. Kapteijn, J. Gascon, O. David, PBI mixed matrix hollow fiber membrane: influence of ZIF-8 filler over H-2/CO2 separation performance at high temperature and pressure, Separ. Purif. Technol. 237 (2020) 116347, https://doi.org/10.1016/j.seppur.2019.116347.
[27] K.M. Gupta, Z.W. Qiao, K. Zhang, J.W. Jiang, Seawater pervaporation through zeolitic imidazolate framework membranes: atomistic simulation study, ACS Appl. Mater. Interfaces 8 (21) (2016) 13392–13399, https://doi.org/10.1021/acsami.6b01626.
[28] S.Y. Chew, S.H. Ng, J.Z. Wang, P. Novak, F. Krumeich, S.L. Chou, J. Chen, H.K. Liu, Flexible free-standing carbon nanotube films for model lithium-ion batteries, Carbon 47 (13) (2009) 2976–2983, https://doi.org/10.1016/j.carbon.2009.06.045.
[29] J.A. Rojas, L.A. Ardila-Rodriguez, M.F. Diniz, M. Goncalves, B. Ribeiro, M. C. Rezende, Optimization of Triton X-100 removal and ultrasound probe parameters in the preparation of multiwalled carbon nanotube buckypaper, Mater. Des. 166 (2019) 107612, https://doi.org/10.1016/j.matdes.2019.107612.
[30] E.P.V. Sanchez, H. Gliemann, K. Haas-Santo, C. Woll, R. Dittmeyer, ZIF-8 SURMOF membranes synthesized by Au-assisted liquid phase epitaxy for application in gas separation, Chem. Ing. Tech. 88 (11) (2016) 1798–1805, https://doi.org/10.1002/cite.201600061.
[31] X.X. Song, B.W. Gan, Z. Yang, C.Y.Y. Tang, C.J. Gao, Confined nanobubbles shape the surface roughness structures of thin film composite polyamide desalination membranes, J. Membr. Sci. 582 (2019) 342–349, https://doi.org/10.1016/j.memsci.2019.04.027.
[32] L. Paseta, D. Antoran, J. Coronas, C. Tellez, 110th anniversary: polyamide/metal-organic framework bilayered thin film composite membranes for the removal of pharmaceutical compounds from water, Ind. Eng. Chem. Res. 58 (10) (2019) 4222–4230, https://doi.org/10.1021/acs.iecr.8b06017.
[33] Y. Liu, L.G. Shen, Z.Y. Huang, J.H. Liu, Y.C. Xu, R.J. Li, M.J. Zhang, H.C. Hong, H. J. Lin, A novel in-situ micro-aeration functional membrane with excellent decoloration efficiency and antifouling performance, J. Membr. Sci. 641 (2022), https://doi.org/10.1016/j.memsci.2021.119925.
[34] B.H. Chen, H.L. Xie, L.G. Shen, Y.C. Xu, M.J. Zhang, H.Y. Yu, R.J. Li, H.J. Lin, Electroless Ni-Sn-P plating to fabricate nickel alloy coated polypropylene membrane with enhanced performance, J. Membr. Sci. 640 (2021), https://doi.org/10.1016/j.memsci.2021.119820.
[35] J.H. Wu, M.J. Xia, Z.W. Li, L.G. Shen, R.J. Li, M.J. Zhang, Y. Jiao, Y.C. Xu, H.J. Lin, Facile preparation of polyvinylidene fluoride substrate supported thin film composite polyamide nanofiltration: effect of substrate pore size, J. Membr. Sci. 638 (2021), https://doi.org/10.1016/j.memsci.2021.119699.
[36] C. Echaide-Gorriz, M. Malankowska, C. Tellez, J. Coronas, Nanofiltration thin-film composite membrane on either the internal or the external surface of a polysulfone hollow fiber, AIChE J. 66 (6) (2020), https://doi.org/10.1002/aic.16970.
[37] G.H. Yang, D.Q. Zhang, G. Zhu, T.R. Zhou, M.T. Song, L.L. Qu, K.C. Xiong, H.T. Li, A Sm-MOF/GO nanocomposite membrane for efficient organic dye removal from wastewater, RSC Adv. 10 (14) (2020) 8540–8547, https://doi.org/10.1039/d0ra01110j.
[38] Y.X. Yao, C.Y. Ba, S.S. Zhao, W.H. Zheng, J. Economy, Development of a positively charged nanofiltration membrane for use in organic solvents, J. Membr. Sci. 520 (2016) 832–839, https://doi.org/10.1016/j.memsci.2016.08.041.
[39] J.N. Krishnan, K.R. Venkatachalam, O. Ghosh, K. Jhaveri, A. Palakodeti, N. Nair, Review of thin film nanocomposite membranes and their applications in

desalination, Front. Chem. 10 (2022), https://doi.org/10.3389/fchem.2022.781372.
[40] V. Freger, Nanoscale heterogeneity of polyamide membranes formed by interfacial polymerization, Langmuir 19 (11) (2003) 4791–4797, https://doi.org/10.1021/la020920q.
[41] M.Q. Seah, W.J. Lau, P.S. Goh, H.H. Tseng, R.A. Wahab, A.F. Ismail, Progress of interfacial polymerization techniques for polyamide thin film (Nano)Composite membrane fabrication: a comprehensive review, Polymers 12 (12) (2020) 2817, https://doi.org/10.3390/polym12122817.
[42] R. Oizerovich-Honig, V. Raim, S. Srebnik, Simulation of thin film membranes formed by interfacial polymerization, Langmuir 26 (1) (2010) 299–306, https://doi.org/10.1021/la9024684.
[43] S.J. Park, W. Choi, S.E. Nam, S. Hong, J.S. Lee, J.H. Lee, Fabrication of polyamide thin film composite reverse osmosis membranes via support-free interfacial polymerization, J. Membr. Sci. 526 (2017) 52–59, https://doi.org/10.1016/j.memsci.2016.12.027.
[44] X. Wang, T.M. Yeh, Z. Wang, R. Yang, R. Wang, H.Y. Ma, B.S. Hsiao, B. Chu, Nanofiltration membranes prepared by interfacial polymerization on thin-film nanofibrous composite scaffold, Polymer 55 (6) (2014) 1358–1366, https://doi.org/10.1016/j.polymer.2013.12.007.
[45] V. Freger, G.Z. Ramon, Polyamide desalination membranes: formation, structure, and properties, Prog. Polym. Sci. 122 (2021), https://doi.org/10.1016/j.progpolymsci.2021.101451.
[46] C. Van Goethem, R. Verbeke, M. Pfanmoller, T. Koschine, M. Dickmann, T. Timpel-Lindner, W. Egger, S. Bals, I.F.J. Vankelecom, The role of MOFs in Thin-Film Nanocomposite (TFN) membranes, J. Membr. Sci. 563 (2018) 938–948, https://doi.org/10.1016/j.memsci.2018.06.040.
[47] L.F. Liu, X. Huang, X. Zhang, K. Li, Y.L. Ji, C.Y. Yu, C.J. Gao, Modification of polyamide TFC nanofiltration membrane for improving separation and antifouling properties, RSC Adv. 8 (27) (2018) 15102–15110, https://doi.org/10.1039/c8ra01374h.
[48] X.N. Wu, L. Yang, F.B. Meng, W.L. Shao, X. Liu, M. Li, ZIF-8-incorporated thin-film nanocomposite (TFN) nanofiltration membranes: importance of particle deposition methods on structure and performance, J. Membr. Sci. 632 (2021) 119356, https://doi.org/10.1016/j.memsci.2021.119356.
[49] D.H. Wu, J. Martin, J.R. Du, Y.F. Zhang, D. Lawless, X.S. Feng, Effects of chlorine exposure on nanofiltration performance of polyamide membranes, J. Membr. Sci. 487 (2015) 256–270, https://doi.org/10.1016/j.memsci.2015.02.021.